



## UvA-DARE (Digital Academic Repository)

### Organic carbon cycling in a Caribbean coral reef

*Hidden biomass, sneezing sponges, and net heterotrophy*

Kornder, N.A.

#### Publication date

2023

[Link to publication](#)

#### Citation for published version (APA):

Kornder, N. A. (2023). *Organic carbon cycling in a Caribbean coral reef: Hidden biomass, sneezing sponges, and net heterotrophy*. [Thesis, fully internal, Universiteit van Amsterdam].

#### General rights

It is not permitted to download or to forward/distribute the text or part of it without the consent of the author(s) and/or copyright holder(s), other than for strictly personal, individual use, unless the work is under an open content license (like Creative Commons).

#### Disclaimer/Complaints regulations

If you believe that digital publication of certain material infringes any of your rights or (privacy) interests, please let the Library know, stating your reasons. In case of a legitimate complaint, the Library will make the material inaccessible and/or remove it from the website. Please Ask the Library: <https://uba.uva.nl/en/contact>, or a letter to: Library of the University of Amsterdam, Secretariat, P.O. Box 19185, 1000 GD Amsterdam, The Netherlands. You will be contacted as soon as possible.



# Chapter

# 5

Carbon cycling in a coral reef: II.  
Do model predictions of organic carbon  
fluxes match *in-situ* community  
measurements?

Niklas A Kornder, Yuki Esser, Lennart J de Nooijer, Alice E Webb, Mark J A Vermeij,  
Jef Huisman, Jasper M de Goeij

In preparation for submission

## ABSTRACT

How coral reefs maintain highly productive communities in an oligotrophic ocean environment is a major enigma that has not yet been fully resolved. For a long time, reef communities were shown to be largely self-sustaining (i.e., balance between gross reef community production and respiration), but recent model studies indicate that present-day reef communities are dominated by consumer species and require oceanic inputs of organic carbon to support their standing biomass. However, these models have not been validated in the field. To address this issue, we incubated six Caribbean benthic reef communities of different taxonomic composition *in situ* and measured their primary productivity, respiration, and uptake/release of plankton, detritus, and dissolved organic carbon. These community-level observations were then compared to the carbon fluxes predicted by (1) a linear-inverse model (LIM) of the incubated communities, and (2) the summed carbon fluxes calculated from controlled incubations of individual taxa and the abundances of these taxa on the reef. The results show that gross primary productivity, respiration, and net fluxes of plankton and detritus were predicted quite well using LIMs. In contrast, net primary productivity was best estimated by summing fluxes of the individual taxa. The measured fluxes of dissolved organic carbon proved hard to predict using either approach, and varied strongly between communities. Our findings improve existing methods to estimate organic carbon fluxes in coral reef communities and corroborate the notion that present-day Caribbean reefs can be sinks of organic carbon.

## INTRODUCTION

The species composition of biological communities is changing rapidly due to anthropogenic activities that have led to, e.g., climate change, ocean acidification, and eutrophication (Mitchell 1989; Smith 2003; Scholze et al. 2006; Guinotte and Fabry 2008). While many changes in community composition have been well documented, often less is known about how these changes affect important ecosystem functions, such as biomass production, carbon storage, and nutrient cycling. Understanding how resources are processed, stored, and recycled in natural communities requires estimation of metabolic activities (e.g., gross primary productivity, respiration), grazing (e.g., herbivory, suspension- or filter-feeding) and predation, and other fluxes of resources (e.g., dissolved organic matter, detritus) among a network of species interactions (e.g., Lotka 1925; Paine 1966; May 1971; Pimm et al. 1991; Mumby and Steneck 2008). Collecting and interpreting such quantitative information is not trivial, but will contribute to a better understanding of how community composition affects ecosystem functioning.

On coral reefs, early studies indicated that metabolic gains from gross primary productivity (GPP) and losses from respiration (R) were very similar. That is, the GPP:R ratio, also referred to as P:R, of coral reef communities was found to be close to one (Margalef 1974; Hatcher 1990; Crossland et al. 1991). In recent decades, reef communities have changed in many areas around the world, undergoing large community shifts (reviewed by Reverter et al. 2022) due to coral mortality from bleaching (Hughes et al. 2017a; Eakin et al. 2019), mass mortalities of sea urchins (Lessios et al. 1984), proliferation of coral predators (Kayal et al. 2012), and the resulting replacement of corals by fleshy algae (McManus and Polsenberg 2004) or sponges (Bell et al. 2013). Such shifts in the abundances of major coral reef taxa are expected to continue throughout the upcoming decades, possibly altering the balance between community production and respiration (Dudgeon et al. 2010; Davis et al. 2021). An improved understanding of how different species affect net fluxes of organic matter (e.g., plankton uptake, turnover of detritus and dissolved compounds) is therefore needed to determine how changes in the composition of coral reef communities affect community metabolism.

In assessments of carbon fluxes in coral reef food webs (reviewed by Bierwagen et al. 2018), estimates of the abundances of functional groups (e.g., corals, fish, algae) are typically multiplied with fluxes of dissolved oxygen and organic matter obtained from incubations of taxa representative of these functional groups (e.g., Chisholm 2003; Schneider et al. 2009). Total community fluxes can then be derived by summing the products of these taxa-specific abundances and fluxes. However, the magnitude of fluxes in coral reef food webs is often not well known or subject to high uncertainty. In this case, linear-inverse models (LIMs) can provide a useful

solution (Christensen and Pauly 1993; Vasconcellos et al. 1997; van Oevelen et al. 2010). In classic ecological models, production and consumption rates and other major fluxes in the community are assumed to be known, and used to predict changes in population abundances of the species. In inverse models, this approach is reversed. The population abundances of the species are measured, and these measurements are used to predict the fluxes within the community. Predictions of presumed fluxes are generally constrained by minimum and maximum values based on measurements to reduce uncertainties and ensure the predictions are bound to realistic values (Opitz 1996; Allesina and Bondavalli 2003; Cáceres et al. 2016). LIMs have improved our quantitative understanding of coral reef food webs (e.g., Christensen and Pauly 1993; Anthony and Fabricius 2000), but have not been validated in the field. Model validation requires measurements of *in-situ* community fluxes within defined benthic coral reef segments to enable direct comparisons between model predictions and field observations, preferably for a variety of reef communities that differ in species composition.

In recent years, ecologists further developed technologies to measure GPP, R, and net fluxes of organic carbon (C) in coral reef communities. Seawater exchange can be tightly regulated in fixed *in-situ* flume tanks (Kline et al. 2012). However, building flume tanks demands significant resources (Srednick et al. 2020) and they cannot be easily deployed on coral reefs. A more cost-effective method is the use of portable benthic “tent” enclosures (described in Haas et al. 2013). These enclosures can be easily folded up and moved to new locations, and their ease of deployment provides the opportunity to measure net C fluxes for semi-isolated (i.e., some seawater exchange persists through the benthos), m<sup>2</sup>-sized patches of reef representing the diversity and complexity of natural reef communities (van Heuven et al. 2018; Roth et al. 2019; Roth et al. 2021). Compared with completely closed incubators, these semi-open enclosures decrease the risks of incubation effects, such as food limitation, or built-up of waste products that could potentially alter the metabolism of the incubated communities. However, as such enclosures are subject to intrusion of ambient seawater affecting the interior concentrations of the measured compounds, estimates of metabolic rates need to be corrected accordingly when using this methodology.

The goal of this study is twofold. First, we aim to validate the predictions of the LIM presented in Chapter 4 against C fluxes of different benthic communities measured *in situ* on the reef. For this purpose, we used benthic tent enclosures on the fringing reef of the Caribbean island of Curaçao to measure GPP and R of the reef community as well as daily fluxes of planktonic, detrital and dissolved organic carbon for six reef patches (hereafter referred to as “reef segments”) that differed in benthic community composition (Figure 1). The predictions of the LIM were constrained by minimum and maximum values of the C fluxes estimated for

individual coral reef taxa and the mean abundances of these taxa in the benthic tents. Second, we compare predictions of the LIM with an alternative approach, in which the average C fluxes by individual taxa were simply multiplied with their abundances in the tents and then summed over all taxa to derive predictions of total C fluxes in the reef community. The results of this study will contribute to more accurate predictions of the metabolic rates and organic C fluxes in coral reef communities and to an improved understanding of how variation in community composition relates to ecosystem functioning on coral reefs.

## METHODS

### C fluxes measured on the reef

#### *In-situ incubations & seawater sampling*

Reef segments (Figure 1) were incubated at 5–16 m depth on the leeward reef slope of Curaçao (Southern Caribbean), directly East of the inlet to Piscadera Bay (12°12'N, 68°56'W) between the 14<sup>th</sup> of February and 21<sup>st</sup> of March 2019 using SCUBA. Benthic organisms were carefully transplanted from adjacent sites at similar depths and placed in the reef segment, in order to adjust the community composition. In total, we incubated one segment in which the biomass was dominated by scleractinian corals (termed “Coral 1”; coral biomass = 79 % of total), three segments containing a mixed benthic community (“Mixed 1, 2, 3”; coral biomass between 40–53 % of total) and two segments where coral biomass was low (18–25 %) and the community biomass was dominated by a large specimen of the sponge *Aplysina archeri* (“Sponge 1, 2”; sponge biomass = 72–78 % of total). Other benthic organisms in these reef segments included calcifying algae and non-calcifying algae (i.e., macroalgae, turf algae, benthic cyanobacterial mats), both less than 10 % of total biomass, and some gorgonians (Tables S1, S2).

To estimate the biomass (in g ash-free dry weight (AFDW)) of the different benthic organisms, the total 3D surface cover of benthic organisms (in cm<sup>2</sup> per tent) in each incubated community was determined by analyzing scaled photographs of all accessible surfaces using the *framing tool* in ImageJ (version 1.X) (Schneider et al. 2012). The same tool was used to quantify the biovolumes of massive sponges and gorgonians in cm<sup>3</sup> tent<sup>-1</sup> by approximating their closest geometrical shape as previously described in Chapter 2 (Kornder et al. 2021). Surface cover and biovolumes were then converted to AFDW using published conversion factors (Kornder et al. 2021).

We used the tetrahedron-shaped semi-enclosed benthic tents described in (Webb et al. 2021) to incubate the reef segments, confining a planar reef area of 0.43 m<sup>2</sup> in 90–119 L of seawater, depending on the volume of the incubated reef community. Each reef segment was incubated for 3–4 h during the day (starting

time between 10:20–11:30) and at night (starting time between 18:58–20:18, Tables S3, S4). The tents were equipped with a continuously running, brushless, submersible water pump (BLDC pump Co., Ltd; flow rate: 40 L h<sup>-1</sup>) to generate water mixing within the tent. During sampling, the water flow generated by the pump was temporarily redirected through an attached gas-impermeable tubing that protruded outside the tent. At the start, after ~1 h, and at the end of each incubation (see Table S2 for exact time intervals), acid-washed (0.4 mol L<sup>-1</sup> HCl) syringes (100 mL) were attached to the tubing, slowly filled, and flushed three times before collecting samples for analysis of the interior concentration of dissolved organic carbon (DOC, in  $\mu\text{mol C L}^{-1}$ ) and abundances of bacterioplankton and phytoplankton (*Prochlorococcus* and *Synechococcus*) (all in cells mL<sup>-1</sup>). Larger samples (4 L) were slowly collected into custom-made seawater sampling cores (described as “Hattay Niskin” in Haas et al. 2014) to measure concentrations of total particulate organic carbon (POC, in  $\mu\text{mol C L}^{-1}$ ). Seawater samples were also taken at 30 cm distance outside the tent, to calculate the influx and efflux of DOC, detrital C, and bacterio- and phytoplankton carbon (from here on termed “planktonic C”) by seawater leaking into and out of the tent.

In addition, sensors with dataloggers were attached to the structural support rods inside the tent for high-frequency measurement at one-minute intervals of photosynthetically active radiation (PAR) (Odyssey, Dataflow Systems Limited, New Zealand, spectral detection range: 400–700 nm, calibration in air against a Walz instrument, Walz ULM500, Walz GmbH, Effeltrich, Germany), salinity (DST CTD, Star-Oddi, Iceland), oxygen (to determine gross and net community productivity and respiration rates), and temperature (HOBO Pendant U-26, Onset, USA). The same high-frequency measurements were also made outside the tent (at 5 m distance for salinity, and at 30 cm distance for PAR, oxygen and temperature) to calculate the influx and efflux of oxygen by seawater leaking in and out of the tent. Leakage rates (0.56–3.84 L min<sup>-1</sup>; Tables S3, S4) were estimated as described in (Webb et al. 2021) by adding 450 mL of salt-saturated water to the tent interior directly after taking the start sample, and tracking the rate at which salinity decreased to ambient levels.

### **Laboratory analyses**

Seawater samples were processed as described in Chapter 4 of this thesis. Briefly, 4 L of seawater was filtered onto pre-combusted (5 h 550°C) 47 mm GF/F filters (~0.7  $\mu\text{m}$  pore size, Whatman) to quantify POC concentrations in an elemental analyzer (CHNS-EA; Vario El Cube, Elementar, Germany). Additional duplicate seawater samples (20 mL) were filtered through pre-combusted 25 mm GF/F filters (Whatman) and the concentration of DOC in the filtrate was analyzed using a total organic carbon analyzer (TOC-Vcph-TNM-1 autoanalyzer, Shimadzu, Japan)

according to Campana et al. (2021). Abundances of bacterio- and phytoplankton were enumerated on a flow cytometer (CytoFLEX, Beckman Coulter, USA) and converted to planktonic C using published conversion factors (*Synechococcus*: 250 fg C cell<sup>-1</sup>; *Prochlorococcus*: 53 fg C cell<sup>-1</sup>; bacteria: 20 fg C cell<sup>-1</sup>) (Campbell et al. 1994). Detrital C was calculated for each sample by subtracting total planktonic C from POC.

### ***Correction for ambient seawater exchange***

Net fluxes of dissolved oxygen as well as planktonic C, detrital C, and DOC measured inside the tents were corrected for exchange with ambient seawater based on the leakage rates and ambient concentrations during the incubations. For this, the measured concentrations of C inside ( $C_{int}$ ) and outside ( $C_{ext}$ ) of the tent were interpolated by linear regression (e.g., Figure 2A–F). Oxygen evolution was fitted with sixth-order polynomial models to leverage the high temporal resolution (one measurement per min) (Figure 2G,H). All models were forced through their starting concentrations (at  $t = 0$ ).

The correction was based on the assumption that the change of the observed C concentration in the tent ( $\Delta C_{int}$ ) equals the community-mediated change of the C concentration in the tent ( $\Delta C_{com}$ ) plus the net C leakage into the tent:

$$(1) \quad \Delta C_{int} = \Delta C_{com} + \text{leakage},$$

where  $\Delta C_x = C_{x,t+1} - C_{x,t}$  was calculated over a short time interval (i.e., one minute). The net change in C concentration due to leakage into the tent was calculated as:

$$(2) \quad \text{leakage}_t = \frac{F}{V}(C_{ext,t} - C_{int,t}),$$

where  $F$  is the leakage rate (in L min<sup>-1</sup>) and  $V$  is the volume of seawater inside the tent (in L). Thus, the community-mediated change of the C concentration in the tent can be described by:

$$(3) \quad C_{com,t+1} - C_{com,t} = C_{int,t+1} - C_{int,t} - \frac{F}{V}(C_{ext,t+1} - C_{int,t+1}),$$

so that the community-mediated concentration at the next time step can be calculated as:

$$(4) \quad C_{com,t+1} = C_{com,t} + C_{int,t+1} - C_{int,t} - \frac{F}{V}(C_{ext,t+1} - C_{int,t+1}).$$

At the start, the community-mediated C concentration is equivalent to the observed C concentration in the tent, i.e.,  $C_{com,0} = C_{int,0}$ , which simplifies the above equation to:

$$(5) \quad C_{com,1} = C_{int,1} - \frac{F}{V}(C_{ext,1} - C_{int,1}).$$

Inserting Equation (5) into Equation (4), and continued iteration, shows that the community-mediated C concentration in the tent can also be written as the observed C concentration in the tent minus the C leakage summed over all preceding time intervals:

$$(6) \quad C_{com,T} = C_{int,T} - \sum_{t=1}^T \frac{F}{V}(C_{ext,t} - C_{int,t}).$$

The community-mediated C concentrations were linearly regressed against time as described above. Subsequently, the regression slopes ( $s$ , in  $\mu\text{mol C L}^{-1} \text{min}^{-1}$ ) were scaled to community-mediated C fluxes ( $\text{FLUX}_{\text{com}}$  in  $\text{mmol C tent}^{-1} \text{h}^{-1}$ ) by multiplying  $s$  with the total seawater volume in the tent:

$$(7) \quad \text{FLUX}_{\text{com}} = s \cdot V \cdot 0.06,$$

Where the factor 0.06 converts  $\mu\text{mol C min}^{-1}$  to  $\text{mmol C h}^{-1}$ .

Daily community fluxes (in  $\text{mmol C tent}^{-1} \text{d}^{-1}$ ) of planktonic C, detrital C, and DOC were approximated by multiplying the C fluxes per hour determined in the light and in the dark by 12 h, and summing the light and dark estimates assuming a 12:12 h cycle. Due to sample contamination, the detrital C flux could not be reliably determined for one segment (Sponge 2) during the light period, and was therefore substituted with the diurnal detrital C flux obtained for the segment Sponge 1 that had a very similar community composition (Figure 1).

Daily fluxes of GPP, R, and NPP were determined from oxygen production and consumption rates (expressed per hour) as described in Chapter 4. Briefly, oxygen was converted to C using a photosynthetic quotient (i.e., mol  $\text{O}_2$  produced per mol  $\text{CO}_2$  assimilated) of 1.19 during the light period and a respiratory quotient (i.e., mol  $\text{CO}_2$  respired per mol  $\text{O}_2$  consumed) of 0.93 during the dark period (Chapter 4, Table S1). GPP was calculated by adding R and NPP, which were converted from hourly to daily fluxes based on the solar irradiance at the study site (see Equations 1 and 2 in Chapter 4). For this, daytime R was assumed to follow the diurnal PAR trajectory and peak during midday (see Chapter 4 for details). Community R at midday was assumed to be 2.87 times nighttime R, which is the mean of the values used in Chapter 4 to calculate daily GPP and R of corals, macroalgae, sponges, and sediment communities.

### ***C fluxes predicted by the linear-inverse model***

We evaluated the performance of the LIM (Chapter 4) by comparing the community-level predictions of the LIM with the community-level C fluxes measured on the reef (in the benthic tents described above). The original LIM was based on specific C fluxes estimated for individual coral reef organisms representative of the different functional groups on the reef (see Tables 1 and S1 in Chapter 4), and their mean abundances along the leeward reef slope of Curaçao. Here, the model was adjusted by replacing these species abundances with the abundances measured in the tents (Tables S1, S2). The LIM was rerun for each reef segment to generate six C-flow models. Community-level predictions were obtained from these models according to the analysis described in Chapter 4 (see “Model construction & analysis”). However, imports and exports of C in the semi-enclosed tents were defined by the exchange of interior and ambient reef water. Therefore, the mean daily seawater volume flow ( $Q$ , in  $\text{L day}^{-1}$ ) was approximated based on the measured leakage rates ( $F$ , in  $\text{L min}^{-1}$ ) in light and dark incubations:

$$(8) \quad Q = 60 \cdot (12 \cdot F_{\text{light}} + 12 \cdot F_{\text{dark}}).$$

Maximum rates of imported and exported C (minimum rates are zero) were estimated for each reef segment by multiplying  $Q$  with the 97.5-percentile of the measured ambient and interior C concentrations, respectively. In addition, maximum rates of imported DOC into the tents were multiplied with 0.2 to limit external inputs of this C pool to labile carbon components (de Goeij and van Duyl 2007).

### ***C fluxes predicted by summing individual taxa***

Instead of the LIM, we also used a simpler method to predict the C fluxes, by adding up the C fluxes estimated for individual taxa. For this purpose, specific C fluxes were obtained from incubations of individual taxa representative of the different functional groups on the reef (see Tables 1 and S1 in Chapter 4). For each of the six reef segments, specific fluxes of all benthic groups present in that segment were summed in proportion to their abundances to obtain total net C fluxes. Uncertainties were propagated using standard methods (see Equations 5 and 7 in Kornder et al. 2021). The predictions of both the LIM and the summed-fluxes approach were compared against our measurements of the metabolic rates (GPP, R, NPP) and net fluxes of planktonic C, detrital C, and DOC in the six reef segments. The accuracy of the predictions was evaluated for each C flux by plotting the predictions versus measurements, and by calculating the normalized mean absolute error (NMAE) and normalized mean bias (NMB) (both normalized by the average measured flux). All calculations were performed in Excel and the models were run in R (R Core Team 2021) using the package *LIM* (Soetaert and van Oevelen 2009).

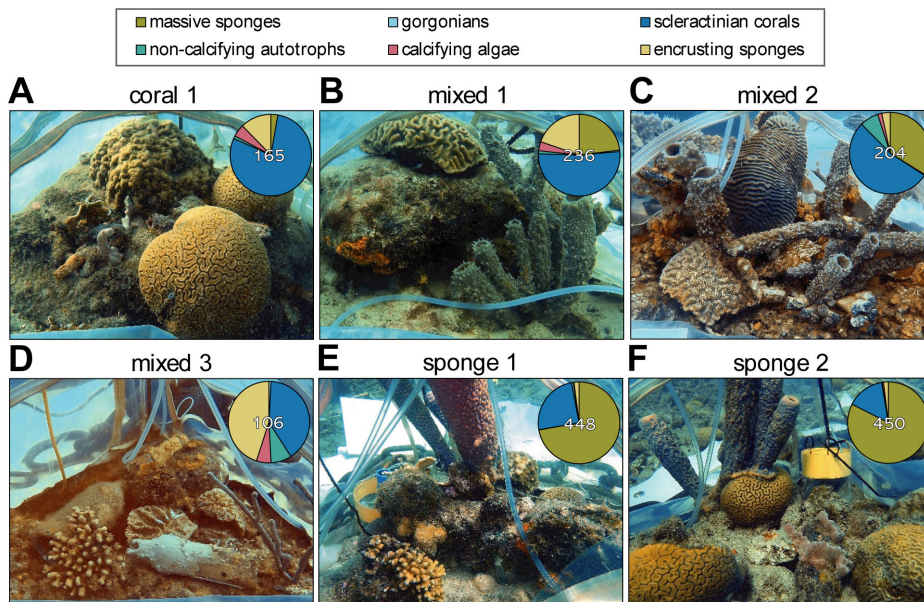


**Figure 1.** Incubated *in-situ* coral reef segments between 5–16 m depth. Pie charts illustrate the composition of the benthic community in each segment. Central white numbers are total biomass in grams ash-free dry weight. Segments were either dominated by scleractinian corals (A), showed a mixed community composition (B–D), or were dominated by sponges (E, F). Communities were incubated for 4–5 h during midday and at night. Further details on community composition and incubation meta-data are given in Tables S1–S4.

## RESULTS

### Correction for ambient seawater exchange

Changes of C concentrations in the benthic tents due to the activity of reef communities were consistently dampened by exchange between reef water inside and outside of the tents (Figure 2). In some cases, the direction (i.e., uptake or release) of the community-driven C flux after correction for water exchange was even opposite to the change of the C concentration in the benthic tents. For instance, the concentration of DOC in the coral-dominated segment (Coral 1) decreased in the tent during the incubation at midday, suggesting community uptake of DOC (Figure 2A, solid dark line). However, this decrease of the DOC concentration in the tent was partially driven by an even larger decline of the ambient DOC concentration on the reef outside the tent, leaking into the tent at a rate of  $1.6 \text{ L min}^{-1}$ . After correction for this exchange of seawater, the reef community in the tent was in fact estimated to release DOC (Figure 2A, dashed line).

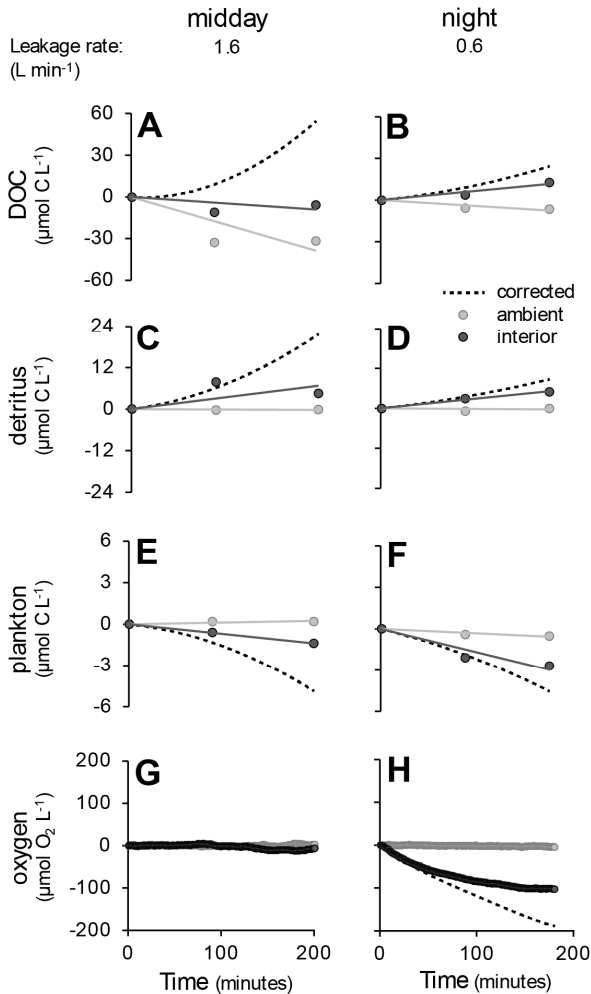


**Figure 2.** Correction for exchange between the ambient and incubated seawater. Shown here are measurements from incubations of the coral-dominated segment (Coral 1) during midday (left panels) and at night (right panels). Concentrations (filled circles) of dissolved organic carbon (A, B), detrital carbon (C, D) and planktonic carbon (E, F) were measured at three time points, while dissolved oxygen (G, H) was measured once per minute. The concentrations in panels A–F were interpolated by linear regression (solid lines) to calculate corrected concentrations (dashed lines) using the specific leakage rates for midday and night incubations.

## Measured versus predicted C fluxes in reef communities

### *Productivity & respiration*

Based on our benthic tent measurements and after correction for ambient seawater exchange, the GPP of the incubated reef communities (107–529 mmol C tent<sup>-1</sup> d<sup>-1</sup>) was consistently lower than R (187–839 mmol C tent<sup>-1</sup> d<sup>-1</sup>; all fluxes presented as minimum and maximum of the mean values of  $n = 6$  benthic reef segments) for all six reef segments. Accordingly, all reef segments were net heterotrophic, with a negative NPP of 64–309 mmol C tent<sup>-1</sup> d<sup>-1</sup> and a P:R ratio of 0.55–0.66 (Table 1).

The LIM generated quite accurate predictions of the magnitude of GPP and R for the reef segments Coral 1, Sponge 2, Mixed 1 and Mixed 3. For these segments, predicted GPP (mean value: 148–227 mmol C tent<sup>-1</sup> d<sup>-1</sup>) was slightly higher than

measured GPP (107–205 mmol C tent<sup>-1</sup> d<sup>-1</sup>, Figure 3A), while predicted R (139–252 mmol C tent<sup>-1</sup> d<sup>-1</sup>) was slightly lower than measured R (187–345 mmol C tent<sup>-1</sup> d<sup>-1</sup>, Figure 3B). Consequently, the range of NPP predicted by the LIM for these four segments (net production of 8 mmol C tent<sup>-1</sup> d<sup>-1</sup> to net consumption of 29 mmol C tent<sup>-1</sup> d<sup>-1</sup>, Figure 3C) was much closer to zero than the measured range of NPP (net consumption of 64–140 mmol C tent<sup>-1</sup> d<sup>-1</sup>). For the segments Sponge 1 and Mixed 2, the measured community GPP, R, and negative NPP were two to three times higher than for the other segments (Table 1), and the LIM predictions were consistently too low (Figure 3A–C).

**Table 1.** Daily and hourly C fluxes measured in the six coral reef segments in the benthic tents. Oxygen was converted to C using photosynthetic and respiratory quotients, and fluxes were corrected for the intrusion of ambient seawater during incubations (see Methods). GPP, gross primary productivity; R, respiration; NPP, net primary productivity; DOC, dissolved organic carbon.

	coral 1	mixed 1	mixed 2	mixed 3	sponge 1	sponge 2	mean	SD
<b>daily rates (mmol C tent<sup>-1</sup> d<sup>-1</sup>)</b>								
GPP	107	142	333	125	529	205	240	164
R	-187	-259	-507	-189	-839	-345	-388	252
P:R	0.57	0.55	0.66	0.66	0.63	0.59	0.61	0.05
NPP	-80.6	-116	-174	-63.9	-309	-140	-147	88.7
DOC	23.3	84.0	58.0	4.18	-18.6	-8.94	23.7	40.1
detrital C	8.96	18.8	3.46	3.55	3.39	5.48	7.27	6.03
planktonic C	-2.83	-3.50	-13.6	-2.41	-5.89	-3.65	-5.31	4.23
particulate C	6.12	15.3	-10.2	1.13	-2.50	1.82	1.95	8.50
bacteria	-1.17	-2.47	-5.79	-0.53	-2.73	-1.91	-2.44	1.84
phytoplankton	-1.66	-1.03	-7.80	-1.88	-3.16	-1.74	-2.88	2.51
<b>hourly rates at midday (μmol C tent<sup>-1</sup> h<sup>-1</sup>)</b>								
converted O <sub>2</sub>	-569	-163	-7856	-3014	-9902	-2293	-3966	4002
DOC	1300	6065	-41.1	550	875	260	1502	2284
detrital C	517	1175	-56.2	114	231	121	350	446
planktonic C	-116	-176	-477	-26.4	-244	-125	-194	156
particulate C	401	998	-534	87.4	-12.4	-4.30	156	511
bacteria	-49.3	-207	-228	18.0	-113	-80.2	-110	94.0
phytoplankton	-66.7	30.9	-249	-44.4	-131	-45.6	-84.3	96.0
<b>hourly rates at night (μmol C tent<sup>-1</sup> h<sup>-1</sup>)</b>								
converted O <sub>2</sub>	-5012	-6928	-13591	-5054	-22477	-9258	-10387	6738
DOC	641	932	4875	-202	-2423	-1006	470	2476
detrital C	230	389	344	182	51.54	336	255	126
planktonic C	-120	-116	-656	-175	-247	-179	-249	205
particulate C	110	273	-312	7.22	-196	156	6.48	222
bacteria	-48.2	0.81	-255	-62.4	-114	-79.3	-93.1	88.0
phytoplankton	-71.4	-117	-401	-112	-133	-99.8	-156	122

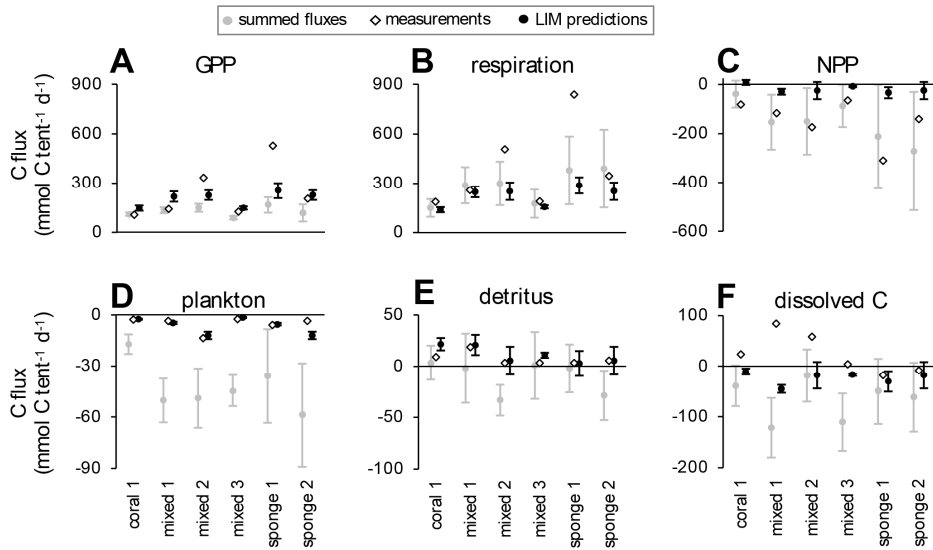


**Figure 3.** Comparison of measured C fluxes (open diamonds) and corresponding predictions (circles, mean  $\pm$  SD). Panels show gross primary productivity (A), respiration (B), net primary productivity (C), and net fluxes of planktonic (D), detrital (E), and dissolved organic carbon (F) in the coral-dominated reef segment, the three mixed reef segments, and the two sponge-dominated reef segments. Predictions were calculated by the LIM (black circles) and by the summed fluxes over individual taxa (grey circles).

The “summed fluxes” approach also generated quite accurate predictions of the magnitude of GPP and R for the segments Coral 1, Sponge 2, Mixed 1 and Mixed 3. Community GPP predicted for these four segments (89–135 mmol C tent<sup>-1</sup> d<sup>-1</sup>) was lower than measured GPP (Figure 3A), while predictions of R (150–390 mmol C tent<sup>-1</sup> d<sup>-1</sup>) were in good agreement with measured R (Figure 3B). The high GPP and R of the segments Sponge 1 and Mixed 2 were underestimated by the summed fluxes (Figure 3A,B). The NPP predicted by the summed fluxes method showed substantial variation, as shown by the large standard deviations for all six reef segments, but this variation captured the NPP of the measurements (Figure 3C).

The performance of the LIM and the summed fluxes approach were evaluated in further detail by regression analysis of the predictions versus measurements, and by calculation of the NMAE and NMB (Figure 4; Table 2). The regression slopes for GPP and R were smaller than 1 and their NMBs were all negative, indicating that both prediction methods strongly underestimated the measured GPP and R. This can be attributed to the high GPP and R measured in reef segments Sponge 1 and Mixed 2, which were not captured by the predictions of the LIM and summed fluxes (Figure 3A,B). When these two segments were excluded from the analysis,

the NMBs were closer to zero (NMB of GPP: 0.11 for LIM and -0.09 for summed fluxes; NMB of R: -0.08 for LIM and 0.11 for summed fluxes), and hence there was no systematic bias in the predictions of GPP and R for the other four reef segments. The NMAEs indicate that the predictions of GPP and R had a similar accuracy for the LIM and the summed fluxes. However, NPP was more accurately predicted by the summed fluxes (lower NMAE and near-zero NMB) than by the LIM (Table 2).

**Table 2.** Prediction performance of the LIM and the summed fluxes method, for each of the investigated C fluxes. Slopes and  $R^2$  values are derived from linear regressions of the predictions versus measurements plotted in Figure 4. The normalized mean absolute error (NMAE) represents the mean deviation between predictions and measurements, while the normalized mean bias (NMB) captures the mean bias in the predictions (i.e., under- or overestimation of the measurements). GPP, gross primary productivity; R, respiration; NPP, net primary productivity; DOC, dissolved organic carbon.

flux	slope		R2		NMAE		NMB	
	model	summed	model	summed	model	summed	model	summed
GPP	0.21	0.15	0.60	0.73	0.45	0.54	-0.15	-0.47
R	0.19	0.28	0.60	0.49	0.49	0.42	-0.43	-0.28
NPP	0.12	0.55	0.48	0.34	0.88	0.45	-0.87	0.03
plankton	0.71	0.73	0.43	0.05	0.45	5.77	0.20	7.01
detritus	1.06	0.91	0.61	0.11	0.48	2.41	0.53	-2.42
DOC	-0.14	-0.21	0.20	0.04	1.86	3.05	-1.98	-3.82

### *Net fluxes of planktonic, detrital, & dissolved organic carbon*

All six reef segments were sinks of planktonic C (2–14 mmol C tent<sup>-1</sup> d<sup>-1</sup>; Figure 3D) and sources of detrital C (3–19 mmol C tent<sup>-1</sup> d<sup>-1</sup>; Figure 3E). Net fluxes of DOC were more variable. DOC consumption (9–19 mmol C tent<sup>-1</sup> d<sup>-1</sup>) was measured in the two reef segments dominated by sponges, while net DOC production (4–84 mmol C tent<sup>-1</sup> d<sup>-1</sup>) was measured in the other four reef segments, particularly in segments Mixed 1 and Mixed 2 (Figure 3F; Table 1).

The LIM generated accurate predictions of the planktonic C consumed (mean predictions: 2–12 mmol C tent<sup>-1</sup> d<sup>-1</sup>, n = 6) and detrital C produced (3–22 mmol C tent<sup>-1</sup> d<sup>-1</sup>) by all six reef segments (Figure 3D,E). However, the LIM predicted net consumption of DOC in all reef segments (11–45 mmol C tent<sup>-1</sup> d<sup>-1</sup>), which was an accurate prediction for the sponge-dominated segments, but missed the net DOC release observed in the coral-dominated and mixed communities (Figure 3F, Figure 4C).

The summed fluxes approach predicted much larger removal rates of planktonic C by the reef communities (17–59 mmol C tent<sup>-1</sup> d<sup>-1</sup>) than observed in our measurements (Figure 3D). Predictions of detrital C released by the segments Coral 1 and Mixed 3 (1–4 mmol C tent<sup>-1</sup> d<sup>-1</sup>) were slightly lower than the measured

release in these two segments (Figure 3E). The summed fluxes deviated from the measured release of detrital C in the four other segments, and instead predicted net consumption of detrital C ( $2\text{--}33 \text{ mmol C tent}^{-1} \text{ d}^{-1}$ ). The summed fluxes approach correctly predicted net consumption of DOC in the two sponge-dominated segments, but did not capture the net DOC release in the other four reef segments (Figure 3F, Figure 4D).

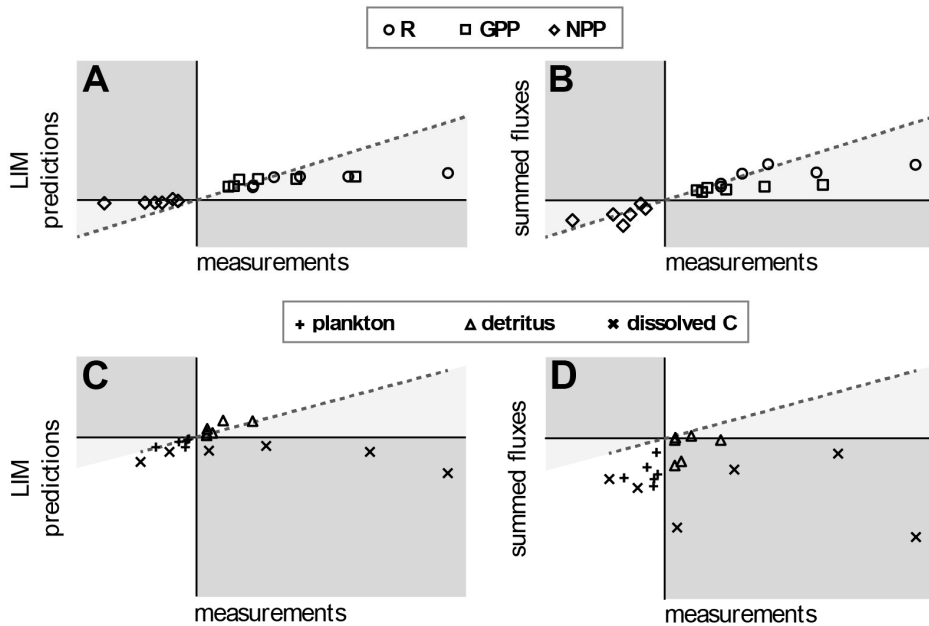


**Figure 4.** Visual assessment of the accuracy of predicted metabolic rates (A, B) and organic matter fluxes (C, D) of coral reef communities. The graphs show the C fluxes predicted by the LIM (A, C) and by the summed fluxes method (B, D) plotted against the measured C fluxes, for all six reef segments. Dashed grey lines indicate perfect fit (i.e., predicted fluxes = measured fluxes). Background shading indicates whether the predicted fluxes tend to be too high (white background), too low (light grey background), or pointing in the wrong direction (dark grey background). Slopes and  $R^2$  values of the linear regression of predictions versus measurements are given in Table 2. R, respiration; GPP, gross primary productivity; NPP, net primary productivity.

Overall, the LIM predicted the amount of planktonic C consumed and detrital C produced by the reef segments much better than the summed fluxes, generating 5–9 times higher  $R^2$  values and 5–13 times lower NMAEs (Table 2). Only a small positive bias was quantified for both particulate C fluxes using the LIM (NMB: 0.2 for planktonic C and 0.5 for detrital C), while the summed fluxes generated highly

erroneous predictions for the consumption of planktonic C (NMB = 7). The regression slopes and NMBs indicate a strong negative bias in all predicted DOC fluxes (Table 2), regardless of the approach (Figure 3F, Figure 4). We suspect that this bias is a result of unaccounted release of DOC in four segments, particularly the segments Mixed 1 and Mixed 2, which harbored individuals of the massive sponge *Callyspongia vaginalis*.

## DISCUSSION

The application of linear-inverse models in ecology (method developed by Soetaert and van Oevelen 2009) facilitates quantifications of community metabolism and biogeochemical fluxes in complex food webs. However, collecting such ecological and biogeochemical data is a daunting task, and hence the predictions of many ecological LIMs lack validation in the field. Here, we compared *in-situ* measurements of the C fluxes in confined coral reef segments (Figure 1) against the predictions of a LIM (Figure 3, Figure 4A,C) and against a simpler method based on the summed C fluxes of individual taxa weighted by their relative abundances on the reef (the “summed fluxes” approach, Figure 4B,D). A key difference between the LIM and the summed fluxes method is that the LIM assumes that the fluxes of different taxa are connected in a large species network and the entire reef community is at steady state (i.e., C inflows and C outflows are in balance). The summed-fluxes method assumes that the fluxes of the different taxa are independent of each other and not necessarily at steady state.

Our results show that the LIM achieved accurate predictions of the net fluxes of planktonic and detrital C in all six reef incubations, while the predictions of community-level GPP and R were also comparable to corresponding *in-situ* measurements in four of the six reef segments. Moreover, the fluxes of planktonic and detrital C predicted by the LIM were more accurate than those obtained by the summed fluxes method (Figure 3D,E, Figure 4B,D, Table 2). However, this was not the case for community NPP, which was skewed towards zero in the LIM predictions (Figure 3C, Figure 4A). Net fluxes of DOC varied strongly across the incubated reef segments, where species-specific differences exceeding the taxonomic resolution of our model can explain deviations of our predictions from the measured DOC fluxes.

Our measurements show that NPP was negative in all six reef segments, including the segment that was dominated by scleractinian corals (Coral 1). This is in good agreement with the earlier results in Chapter 4 and provides additional support for the net heterotrophic nature of these reef communities. However, the LIM predicted a slightly positive NPP for the segment Coral 1 and underestimated the negative NPP of the other segments by up to one order of magnitude (Figure 3C). This implies that the reef communities were even more heterotrophic than

suggested by the LIM analysis in Chapter 4. Most likely, community NPP was skewed towards zero as a result of the steady-state assumption of the LIM, which enforces a close balance between the magnitudes of GPP and R in the model predictions. The summed fluxes method yielded more accurate predictions of the measured NPP. Our results therefore suggest that it is more appropriate to simply sum the NPP of the individual taxa—rather than to balance their C inputs and outputs in LIMs—to estimate NPP at the community level.

Both the LIM and summed fluxes captured the net DOC consumption in the sponge-dominated communities, whereas both methods underestimated the observed net release of DOC in mixed and coral-dominated reef communities (Figure 3F). Release of DOC was strongest in the two mixed reef segments containing large individuals of the low-microbial abundance sponge *Callyspongia vaginalis* (Figure 1, segments Mixed 1 and Mixed 2). *In-situ* measurements of C fluxes by *C. vaginalis* and another closely related species (McMurray et al. 2018) showed that these sponges released DOC at very high rates ( $4.8 \pm 3.3 \text{ mmol C dm}^{-3} \text{ h}^{-1}$ ,  $n = 3$ ), which contrasts to the net DOC uptake by other Caribbean sponges (massive growth form, uptake rates:  $0.3 \pm 0.6 \text{ mmol C dm}^{-3} \text{ h}^{-1}$ , mean  $\pm$  SD,  $n = 17$ , encrusting growth form, uptake rates:  $0.1\text{--}0.2 \text{ mmol C cm}^{-2} \text{ h}^{-1}$ ,  $n = 38$ ) (de Goeij et al. 2008b; McMurray et al. 2018; Hudspith et al. 2022). It is interesting to note that the published DOC release rates for *Callyspongia* spp. in McMurray et al. (2018) were removed as outliers during parameterization of the LIM, and consequently did not contribute to constraining C fluxes through massive sponges in our LIM predictions. In total, our findings highlight that sponges often have a strong impact on DOC fluxes in reef communities. We conclude that the categorization of sponges into species of massive versus encrusting growth forms was likely too broad in light of their diverse nutritional strategies (McMurray et al. 2018), which affected whether our incubated reef segments were sources or sinks of DOC (Figure 3E).

Although our results show good agreement between measurements and LIM predictions of the total daily GPP, R, and net fluxes of planktonic and detrital C in most of the incubated reef segments, our *in-situ* flux measurements can be improved by increasing the temporal resolution of discrete sampling. This becomes evident when examining the effect of our mathematical correction on the concentration of dissolved oxygen (Figure 2G,H), which was measured in high frequency (one measurement per minute). The concentration of dissolved oxygen decreased initially in all night incubations, creating a concentration difference between interior and ambient seawater that became larger as more oxygen was consumed by the incubated fauna. When the intrusion of ambient oxygen matched its consumption by the benthic community within the tent after about 150 min, the interior oxygen concentration remained constant (solid black line in Figure 2H), whereas the flux obtained after correcting for seawater exchange showed

continuous uptake of oxygen (dashed line in Figure 2H), as one would expect from *in-situ* nighttime community R (Long et al. 2013). In contrast, our corrected concentrations of detrital, planktonic, and dissolved organic C changed at an exponential instead of a linear rate throughout the incubations, especially when seawater exchange was relatively high (i.e.,  $>1 \text{ L min}^{-1}$ ) (dashed lines in Figure 2A,C,E). This was an artefact of the linear interpolation of only three discrete measurements of the detrital, planktonic, and dissolved organic C concentrations, on which the corrections were based (see Figure 2). Increasing the frequency of sampling would probably improve our correction of these C fluxes.

In conclusion, our results show that LIMs can predict C fluxes in coral reef communities with reasonable accuracy, especially the net fluxes of particulate C in the form of plankton and detritus, and to a lesser extent also the C fluxes due to community GPP and R. However, the LIMs consistently underestimated negative rates of community-level NPP by assuming that reef communities are in steady state, highlighting the need to combine models with *in-situ* measurements of the net community metabolism on coral reefs. The *in-situ* measurements corroborate the hypothesis that some present-day Caribbean coral reefs are net heterotrophic, supported by uptake of plankton and dissolved organic carbon from oceanic waters above the reef. Our analysis also outlines the dominant role of sponges in mediating reef community fluxes of DOC, the largest flux of organic carbon on reefs. As demonstrated here, the combination of mathematical models and *in-situ* incubations of benthic reefs can contribute to a better understanding of the functioning of coral reef communities, and their role in the processing of marine organic carbon.

### **Acknowledgements**

We thank Benjamin Mueller, Beatriz Pereira, Didier de Bakker, as well as the Carmabi Research Foundation for their support during fieldwork. We also thank Eva de Rijke and Rutger van Hall for their support in the laboratory. This work was funded by the European Research Council under the European Union's Horizon 2020 research and innovation programme (Starting Grant agreement # 715513 to JMdG).

## SUPPLEMENTARY INFORMATION

## Supplementary tables

**Table S1.** Volume of the substrate and volume and biomass of massive sponges and gorgonians in the six incubated reef segments. Conversion factors were obtained from Kornder et al. (2021). Bold groups depict sums of underlying subgroups or species. AFDW, ash-free dry weight.

reef segment	group / species	volume [cm <sup>3</sup> ]	conversion [g <sub>AFDW</sub> cm <sup>-3</sup> ]	biomass [g <sub>AFDW</sub> ]	biomass [% of total]
Coral 1	reef substrate	28210			
	<b>massive sponges</b>	48.1		4.53	2.75
	<i>Aplysina archeri</i>	39.0	0.1058	4.13	2.51
	<i>Desmapsamma anchorata</i>	9.14	0.0439	0.40	0.24
	<b>gorgonians</b>	0.00		0.00	0.00
Mixed 1	reef substrate	23408			
	<b>massive sponges</b>	1131		54.2	23.00
	<i>Callyspongia vaginalis</i>	924	0.0374	34.5	14.67
	<i>Aplysina lacunosa</i>	131	0.1165	15.3	6.49
	<i>Desmapsamma anchorata</i>	47.3	0.0439	2.08	0.88
	unidentified	28.1	0.0804	2.26	0.96
	<b>gorgonians</b>	34.2		1.35	0.57
	<i>Eunicea sp.</i>	34.2	0.0393	1.35	0.57
Mixed 2	reef substrate	9018			
	<b>massive sponges</b>	44.0		68.8	33.82
	<i>Callyspongia vaginalis</i>	44.0	0.0374	68.8	33.82
	<b>gorgonians</b>	14.7		0.58	0.28
	<i>Eunicea sp.</i>	14.7	0.0393	0.58	0.28
Mixed 3	reef substrate	485			
	cavities	1915			
	<b>massive sponges</b>	0.00		0.00	0.00
	<b>gorgonians</b>	22.5		0.88	0.84
	<i>Eunicea sp.</i>	22.5	0.0393	0.88	0.84
Sponge 1	reef substrate	19908			
	<b>massive sponges</b>	3056		323	72.28
	<i>Aplysina archeri</i>	3056	0.1058	323	72.28
	<b>gorgonians</b>	0		0	0.00
Sponge 2	reef substrate	18868			
	<b>massive sponges</b>	3370		352	78.17
	<i>Aplysina archeri</i>	3295	0.1058	348	77.45
	<i>Desmapsamma anchorata</i>	74.6	0.0439	3.28	0.73
	<b>gorgonians</b>	0		0.00	0.00

**Table S2.** Surface area of the substrate and surface area and biomass of benthic reef organisms (except massive sponges and gorgonians) in the six incubated reef segments. Areal densities were obtained from Kornder et al. (2021). Bold groups depict sums of underlying subgroups or species. AFDW, ash-free dry weight.

reef segment	group / species	3D surface area [cm <sup>2</sup> ]	conversion [gAFDW cm <sup>-2</sup> ]	biomass [gAFDW]	biomass [% of total]
Coral 1	reef substrate	5519			
	<b>scleractinian corals</b>	1469		130	78.90
	<i>Porites astreoides</i>	538	0.0142	7.62	4.63
	<i>Diploria labyrinthiformis</i>	861	0.1369	118	71.65
	<i>Millepora alcornis</i>	68.0	0.0617	4.19	2.55
	<i>Siderastrea radians</i>	1.98	0.0617	0.12	0.07
	<b>non-calcifying autotrophs</b>	1011		1.84	1.12
	<i>Lobophora spp.</i>	117	0.0067	0.78	0.47
	turf algae	797	0.0013	1.03	0.63
	benthic cyanobacterial mats	96.9	0.0004	0.04	0.02
	<b>calcifying algae</b>	626		8.10	4.93
	<b>encrusting sponges</b>	478		20.2	12.30
	<i>Scopalina ruetzleri</i>	15.0	0.0404	0.61	0.37
	unidentified	463	0.0424	19.6	11.93
	<b>mixed cryptic communities</b>	950			
	<b>coral rock communities</b>	592			
<b>sediment</b>	393				
Mixed 1	reef substrate	9136			
	<b>scleractinian corals</b>	1184		122	51.95
	<i>Siderastrea siderea</i>	11.9	0.0095	0.11	0.05
	<i>Agaricia sp.</i>	157	0.0962	15.1	6.43
	<i>Stephanocoenia intersepta</i>	424	0.0617	26.2	11.10
	<i>Colpophyllia natans</i>	591	0.1369	80.9	34.37
	<b>non-calcifying autotrophs</b>	1950		2.89	1.23
	<i>Dictyota spp.</i>	496	0.0026	1.29	0.55
	turf algae	1154	0.0013	1.49	0.63
	benthic cyanobacterial mats	300	0.0004	0.11	0.05
	<b>calcifying algae</b>	653	0.0129	8.45	3.59
	<b>encrusting sponges</b>	1105		46.3	19.67
	<i>Scopalina ruetzleri</i>	276	0.0404	11.1	4.73
	unidentified	830	0.0424	35.2	14.93
	<b>mixed cryptic communities</b>	1286			
	<b>coral rock communities</b>	771			
<b>sediment</b>	2186				
Mixed 2	reef substrate	5763			
	<b>scleractinian corals</b>	1027		109	53.44
	<i>Stephanocoenia intersepta</i>	140	0.0617	8.61	4.23
	<i>Colpophyllia natans</i>	591	0.1369	80.9	39.76
	<i>Meandrina meandrites</i>	75.0	0.0617	4.62	2.27
	<i>Eusmilia fastigiata</i>	222	0.0659	14.6	7.17
	<b>non-calcifying autotrophs</b>	2674		15.2	7.45
	<i>Lobophora spp.</i>	2183	0.0067	14.5	7.14
	turf algae	492	0.0013	0.63	0.31
	<b>calcifying algae</b>	271		3.29	1.62
	crustose coralline algae	241	0.0129	3.12	1.53

## Carbon cycling in coral reefs: II. Model validation

reef segment	group / species	3D surface area [cm <sup>2</sup> ]	conversion [gAFDW cm <sup>-2</sup> ]	biomass [gAFDW]	biomass [% of total]
	<i>Halimeda sp.</i>	30.1	0.0056	0.17	0.08
	<b>encrusting sponges</b>	162	0.0424	6.89	3.38
	<b>mixed cryptic communities</b>	1172			
	<b>coral rock communities</b>	456			
	<b>sediment</b>	0			
Mixed 3	reef substrate	6591			
	<b>scleractinian corals</b>	433		42.3	40.11
	<i>Eusmilia fastigiata</i>	150	0.0659	9.90	9.38
	<i>Siderastrea radians</i>	10.2	0.0617	0.63	0.60
	<i>Colpophyllia natans</i>	200	0.1369	27.3	25.88
	<i>Meandrina meandrites</i>	72.9	0.0617	4.49	4.26
	<b>non-calcifying autotrophs</b>	2461		8.68	8.22
	<i>Dictyota spp.</i>	437	0.0026	1.14	1.08
	<i>Lobophora spp.</i>	967	0.0067	6.44	6.10
	turf algae	774	0.0013	1.00	0.95
	benthic cyanobacterial mats	282	0.0004	0.11	0.10
	<b>calcifying algae</b>	475		6.75	5.82
	crustose coralline algae	475	0.0129	6.14	5.82
	<i>Amphiroa sp.</i>	52.0	0.0117	0.61	0.58
	<b>encrusting sponges</b>	1126		47.5	45.01
	<i>Scopalina ruetzleri</i>	114	0.0404	4.60	4.35
	unidentified	1013	0.0424	42.9	40.66
	<b>mixed cryptic communities</b>	1110			
	<b>coral rock communities</b>	935			
	<b>sediment</b>	0			
Sponge 1	reef substrate	6330			
	<b>scleractinian corals</b>	1324		110	24.71
	<i>Siderastrea siderea</i>	80.0	0.0095	0.76	0.17
	<i>Millepora complanata</i>	406	0.0617	25.1	5.60
	<i>Madracis mirabilis</i>	233	0.0995	23.2	5.19
	<i>Orbicella faveolata</i>	88.8	0.1379	12.2	2.74
	<i>Siderastrea radians</i>	18.6	0.0617	1.15	0.26
	<i>Porites astreoides</i>	114	0.0142	1.63	0.36
	<i>Madracis decactis</i>	78.0	0.0617	4.81	1.08
	<i>Diploria labyrinthiformis</i>	304	0.1369	41.7	9.32
	<b>non-calcifying autotrophs</b>	1774		3.42	0.76
	<i>Dictyota spp.</i>	924	0.0026	2.40	0.54
	turf algae	762	0.0013	0.98	0.22
	benthic cyanobacterial mats	88.0	0.0004	0.03	0.01
	<b>calcifying algae</b>	77.7	0.0129	1.01	0.22
	<b>encrusting sponges</b>	219	9.0616	9.06	2.03
	<i>Scopalina ruetzleri</i>	114	0.0404	4.62	1.03
	unidentified	104	0.0424	4.44	0.99
	<b>mixed cryptic communities</b>	448			
	<b>coral rock communities</b>	1211			
	<b>sediment</b>	1275			
Sponge 2	reef substrate	4687			
	<b>scleractinian corals</b>	865		82.5	18.33
	<i>Porites astreoides</i>	206	0.0142	2.92	0.65
	<i>Diploria strigosa</i>	237	0.1369	32.5	7.21
	<i>Madracis decactis</i>	21.4	0.0617	1.32	0.29

reef segment	group / species	3D surface area [cm <sup>2</sup> ]	conversion [g <sub>AFDW</sub> cm <sup>-2</sup> ]	biomass [g <sub>AFDW</sub> ]	biomass [% of total]
	<i>Millepora alvicornis</i>	60.3	0.0617	3.72	0.83
	<i>Diploria labyrinthiformis</i>	180	0.1369	24.7	5.49
	<b>non-calcifying autotrophs</b>	1006		1.69	0.37
	<i>Dictyota spp.</i>	404	0.0026	1.05	0.23
	turf algae	346	0.0013	0.45	0.10
	benthic cyanobacterial mats	55.3	0.0004	0.02	0.00
	<b>calcifying algae</b>	460	0.0129	5.95	1.32
	<b>encrusting sponges</b>	192	0.0424	8.13	1.81
	<b>mixed cryptic communities</b>	480			
	<b>coral rock communities</b>	1684			
	<b>sediment</b>	0			

**Table S3.** Properties of light incubations of the six reef segments and associated measurements of organic carbon (C). Concentrations labeled “outside” are concentrations in ambient seawater at 30 cm distance to the incubation enclosure. AFDW, ash-free dry weight.

reef segment	coral 1	mixed 1	mixed 2	mixed 3	sponge 1	sponge 2
date	21/02/19	18/03/19	7/03/19	21/03/19	1/03/19	14/02/19
depth [m]	6.0	5.2	15.0	16.1	6.0	5.1
community volume [L]	28.3	24.6	10.9	-1.4	23.0	22.2
seawater volume [L]	79.7	93.4	107.1	119.4	95.0	95.8
leakage rate [L min <sup>-1</sup> ]	1.6	3.3	3.8	0.8	2.5	1.7
leakage rate [L d <sup>-1</sup> ]	2365	4746	5522	1133	3532	2489
start of incubation	10:50	11:27	10:23	10:20	11:30	11:11
intermediate sample	12:20	13:07	11:53	11:50	13:10	12:40
end of incubation	14:10	14:37	13:28	13:30	14:30	14:50
<b>particulate organic matter [mg<sub>AFDW</sub> L<sup>-1</sup>]</b>						
start	2.0	5.8	5.2	5.0	5.8	
intermediate	4.9	5.1	4.6	4.6	6.3	
end	2.4	4.6	6.1	4.3	9.2	
intermediate outside	1.2	5.1	4.9	4.4	6.9	
end outside	4.9	5.2	4.9	4.8	11.4	
<b>particulate organic carbon [μmol C L<sup>-1</sup>]</b>						
start	8.6	8.2	9.7	6.9	9.4	
intermediate	15.8	11.3	7.0	8.0	9.7	
end	11.7	16.7	8.5	8.2	26.0	
intermediate outside	8.5	8.2	14.7	8.4	21.5	
end outside	8.6	8.9	9.2	6.3	26.2	
<b>dissolved organic carbon [μmol C L<sup>-1</sup>]</b>						
start	119.2	121.9	140.4	108.4	88.3	102.1
intermediate	108.1	106.8	127.1	114.0	120.0	105.0
end	113.4	161.7	130.8	114.3	89.8	146.1
intermediate outside	86.5	100.2	126.8	111.6	90.5	116.3
end outside	87.4	99.5	127.0	100.9	99.5	159.8
<b>heterotrophic bacteria [μmol C L<sup>-1</sup>]</b>						
start	1.3	1.5	1.7	0.9	0.9	1.2
intermediate	0.9	0.6	0.5	1.2	0.4	0.4
end	0.6	0.4	0.3	1.2	0.2	0.3

## Carbon cycling in coral reefs: II. Model validation

reef segment	coral 1	mixed 1	mixed 2	mixed 3	sponge 1	sponge 2
intermediate outside	1.4	1.7		0.4	1.2	1.3
end outside	1.2	1.9	1.5	1.2	1.2	
<b>phytoplankton [<math>\mu\text{mol C L}^{-1}</math>]</b>						
start	1.3	1.0	2.1	1.2	1.2	0.6
intermediate	1.1	1.0	0.2	1.4	0.1	0.2
end	0.6	1.1	0.1	0.5	0.1	0.2
intermediate outside	1.5	0.8	0.6	1.5	1.1	0.8
end outside	1.6	0.8	1.5	1.7	1.0	0.8
<b>plankton [<math>\mu\text{mol C L}^{-1}</math>]</b>						
start	2.6	2.4	3.8	2.1	2.0	1.8
intermediate	2.0	1.6	0.6	2.6	0.5	0.6
end	1.2	1.4	0.5	1.6	0.3	0.5
intermediate outside	2.8	2.5		1.9	2.3	2.1
end outside	2.8	2.7	3.1	2.9	2.2	0.8
<b>detritus [<math>\mu\text{mol C L}^{-1}</math>]</b>						
start	6.0	5.8	5.9	4.7	7.4	
intermediate	13.8	9.8	6.4	5.4	9.2	
end	10.6	15.3	8.0	6.5	25.7	
intermediate outside	5.7	5.7		6.5	19.2	
end outside	5.8	6.2	6.1	3.4	24.0	

**Table S4.** Properties of dark incubations of the six reef segments and associated measurements of organic carbon (C). Concentrations labeled “outside” are concentrations in ambient seawater at 30 cm distance to the incubation enclosure. AFDW, ash-free dry weight.

reef segment	coral 1	mixed 1	mixed 2	mixed 3	sponge 1	sponge 2
date	25/02/19	19/03/19	5/03/19	20/03/19	4/03/19	19/02/19
depth [m]	6.0	5.2	15.0	16.1	6.0	5.1
community volume [L]	28.3	24.6	10.9	-1.4	23.0	22.2
seawater volume [L]	79.7	93.4	107.1	119.4	95.0	95.8
leakage rate [ $\text{L min}^{-1}$ ]	0.6	1.6	3.7	1.0	1.7	1.7
leakage rate [ $\text{L d}^{-1}$ ]	811	2366	5382	1498	2384	2468
start of incubation	19:05	19:10	19:10	18:58	19:10	20:18
intermediate sample	20:35	20:40	20:40	20:30	20:40	22:00
end of incubation	22:05	22:10	22:20	22:08	22:10	23:30
<b>particulate organic matter [<math>\text{mg}_{\text{AFDW}} \text{L}^{-1}</math>]</b>						
start	1.5	8.7	5.6	4.6	6.5	1.9
intermediate	6.0	10.5	6.0	4.1	7.0	1.8
end	5.5	4.8	5.4	3.9	5.6	2.5
intermediate outside	3.9	5.6	6.2	4.2	5.8	1.3
end outside	4.3	4.5	4.5	4.1	4.9	1.5
<b>particulate organic carbon [<math>\mu\text{mol C L}^{-1}</math>]</b>						
start	10.7	7.8	14.4	9.5	12.7	10.3
intermediate	11.5	12.3	11.4	8.1	8.3	9.2
end	13.0	11.9	12.6	8.8	10.8	11.2
intermediate outside	9.4	16.5	15.8	7.6	10.8	7.5
end outside	10.2	7.0	12.8	7.3	11.6	8.5

5

reef segment	coral 1	mixed 1	mixed 2	mixed 3	sponge 1	sponge 2
<b>dissolved organic carbon [<math>\mu\text{mol C L}^{-1}</math>]</b>						
start	97.3	116.7	111.6	116.9	116.7	157.9
intermediate	100.9	120.1	144.7	126.5	85.3	103.7
end	110.1	136.2	140.8	111.5	98.0	119.3
intermediate outside	91.5	126.7	129.9	119.8	127.0	101.4
end outside	90.7	122.9	110.3	121.6	112.0	107.0
<b>heterotrophic bacteria [<math>\mu\text{mol C L}^{-1}</math>]</b>						
start	1.8	1.1	1.6	1.2	0.9	1.6
intermediate	1.1	0.8	0.4	0.7	0.2	0.7
end	0.7	1.3	0.3	0.2	0.2	0.8
intermediate outside	1.7	0.7	1.9	1.1	1.5	1.5
end outside	1.8	1.3	1.8	0.9	1.5	1.6
<b>phytoplankton [<math>\mu\text{mol C L}^{-1}</math>]</b>						
start	2.0	2.0	2.6	2.0	1.2	1.8
intermediate	0.6	1.0	0.4	0.8	0.1	0.5
end	0.4	0.7	0.3	0.4	0.1	0.6
intermediate outside	1.7	1.9	2.6	2.1	1.5	1.3
end outside	1.5	1.9	2.5	1.6	1.4	1.5
<b>plankton [<math>\mu\text{mol C L}^{-1}</math>]</b>						
start	3.8	3.1	4.2	3.2	2.1	3.3
intermediate	1.7	1.8	0.8	1.6	0.3	1.2
end	1.1	2.0	0.7	0.6	0.3	1.3
intermediate outside	3.4	2.7	4.5	3.2	3.0	2.8
end outside	3.3	3.2	4.3	2.5	2.9	3.1
<b>detritus [<math>\mu\text{mol C L}^{-1}</math>]</b>						
start	6.9	4.7	10.2	6.3	10.6	6.9
intermediate	9.8	10.5	10.6	6.6	8.1	8.0
end	11.9	10.0	12.0	8.3	10.5	9.8
intermediate outside	6.0	13.9	11.4	4.4	7.8	4.7
end outside	6.9	3.7	8.6	4.8	8.7	5.4

## Supplementary data & code

This chapter contains supplementary data and code, available at [figshare.com](https://figshare.com) (DOI: 10.21942/uva.22592905). Additional requests regarding these resources should be directed to and will be fulfilled by the lead contact, Niklas A. Kornder ([niklaskornder@googlemail.com](mailto:niklaskornder@googlemail.com)).

**Data S1.** Raw measurements of all high-frequency *in-situ* measurements (one measurement per minute) of dissolved  $\text{O}_2$  concentrations and other environmental parameters inside (column denoted as “...IN”) and outside (column denoted as “...OUT”) of the benthic tents during incubations. Each tab list all measurements for a single incubation. Names of tabs correspond with the names of the incubated coral reef communities in Figures 1 and 3 and Table 1 in addition to “light” for incubations performed at midday or “dark” for incubations performed at night.

**Data S2–S7.** Output of the linear-inverse models for the benthic reef segments Coral 1, Mixed 1–3, and Sponge 1 and 2. Each column represents a single flow of C between two compartments of the model and lists all 10000 model solutions for that flow. See Box 1 in Chapter 4 for a description of the abbreviations of the functional groups.

**Code S1–S6.** These R scripts define ranges and relationships for the carbon flows of the linear-inverse models for the benthic reef segments Coral 1, Mixed 1–3, and Sponge 1 and 2. The texts can be saved in R's current directory as "file\_name.input" to rerun the model using Code S1 of Chapter 4. The text behind exclamation marks is purely descriptive. The structural elements of the script are explained in Soetaert & van Oevelen (2009).

**Raw images of benthic communities.** Raw images of the benthic communities Coral 1, Mixed 1–3, and Sponge 1 and 2. The surface areas of benthic organisms were estimated using delineation in ImageJ, and converted to biomass using the conversion factors presented in Chapter 2.